

Criticality of Engine Exhaust Simulations on VSTOL Model-Measured Ground Effects

J. R. Lummus*

General Dynamics, Fort Worth, Texas

An experimental investigation funded by the Office of Naval Research has been conducted which demonstrates the criticality of performing accurate full-scale engine-exhaust simulations during model-measured VSTOL ground-effects testing. The effects of varying the nozzle-exit turbulence, total-pressure distributions, and nozzle-pressure ratio on the net and component ground-induced forces for two-, three-, and four-nozzle configurations were studied. Nozzle-exit turbulence intensities and pressure distributions were determined by exit surveys with a Kulite subminiature-pressure transducer and a total-pressure probe. Screens of varying grid size and plates with varying hole patterns were used to achieve variations in turbulent intensity and pressure distributions (respectively) that are characteristic of real aircraft turbojet and turbofan engines at representative nozzle-pressure ratios ranging from 1.5 to 2.4. Although the magnitude of change was highly configuration dependent, increasing the turbulence intensity in all cases resulted in significantly more-unfavorable ground effects. For planforms characteristic of real aircraft, varying the turbulence from turbojet to turbofan-engine levels with relatively high-bypass ratios (or fans) results in an equivalent 10% lift or thrust loss which is on the order of the payload of the aircraft.

Nomenclature

D, d	= nozzle-exit diameter
F_j	= total isolated thrust of all jet nozzles for single- or multiple-jet configurations
f	= frequency
H, h	= height of the blocking surface above the ground surface
I	= turbulent intensity (based on Kulite pressure measurements in this study)
ΔL	= total induced lift on the blocking surface, equal to the sum of the fountain and suckdown components
ΔL_F	= total incremental effect of the fountain on the induced lift, equal to the sum of the fountain core and fountain interference components
ΔL_{FC}	= lift of the fountain core obtained from integrations of the rake pressure data
ΔL_{FI}	= fountain interference lift
ΔL_j	= pure suckdown obtained with single nozzle
NPR	= nozzle pressure ratio
P_k	= blocking surface designation where k indicates plate used (see Fig. 3)
P_{total}, P_{TP}	= total pressure
P_1, P_2	= pressure distribution plates (see Fig. 4)
r	= radial distance measured across nozzle exit diameter
S	= Strouhal number
S_1	= turbulence screen with element size = 0.125 in. (see Fig. 4)
S_2	= turbulence screen with element size = 0.240 in. (see Fig. 4)
ϵ	= largest physical dimension for turbulence generation; grid size for screens in this experiment
ϵ_e	= average size of turbulent energy-containing eddies of consequence (Kolmogorof ¹⁵)

Introduction

WHEN a VSTOL aircraft operates near the ground, the high-velocity jets exhausting below the aircraft react with the ground and airframe (Fig. 1) to produce propulsion-induced aerodynamic forces and moments which must be determined for accurate propulsion and control-system sizing and, hence, accurate aircraft sizing. Accurate prediction of these induced aerodynamic forces is critical to VSTOL aircraft design because they can represent significant changes in the thrust required for VTOL operations, resulting in large increases in required takeoff-gross weight and, ultimately, in large cost increases to accomplish mission requirements. Research with free jets¹⁻⁴ and recent flight test experience with full-scale aircraft (VAK-191B)⁵ indicate that nozzle-exit conditions influence the magnitude of these induced forces. Therefore, to improve the accuracy of current prediction methodologies and to gain physical understanding of the flow mechanisms involved, an experimental investigation was conducted to determine the criticality of full-scale engine-nozzle exit conditions (nozzle-exit turbulence, total-pressure distribution, and pressure ratio over the ranges expected for full-scale aircraft engines) on the propulsion-induced aerodynamic forces for two-, three-, and four-nozzle configuration models with flat-plate surfaces. This investigation was limited to the case of hover in still air (no crosswind, no forward speed) with zero pitch, yaw and roll angle.

The net-induced normal force on the aircraft, ΔL , is the summation of two oppositely directed forces, suckdown and fountain [see Eq. (1)]. Suckdown ΔL_j is a negative force (lift loss) produced by suction pressures on the underside of the airplane created by large quantities of air entrained by the turbulent exhaust and ground jets below the aircraft. The fountain occurs when two or more engine-exhaust jets impinge on the ground plane and the resulting radially expanding ground jets meet to form a vertical-upflow region or fountain. This fountain induces a positive force, ΔL_F , (lift enhancing) to the airplane that sometimes cancels or exceeds the negative suckdown force.

$$(\Delta L/F_j) = (\Delta L_j/F_j) + (\Delta L_F/F_j) \quad (1)$$

It has been shown¹⁰ that the fountain phenomena should be treated as being composed of two separate but additive effects

Presented as Paper 80-0230 at the AIAA 18th Aerospace Sciences Meeting, Pasadena, Calif., Jan. 14-16, 1980; submitted Feb. 5, 1980; revision received June 27, 1980. Copyright © American Institute of Aeronautics and Astronautics, Inc., 1981. All rights reserved.

*Engineering Specialist, Aerospace Technology Dept.

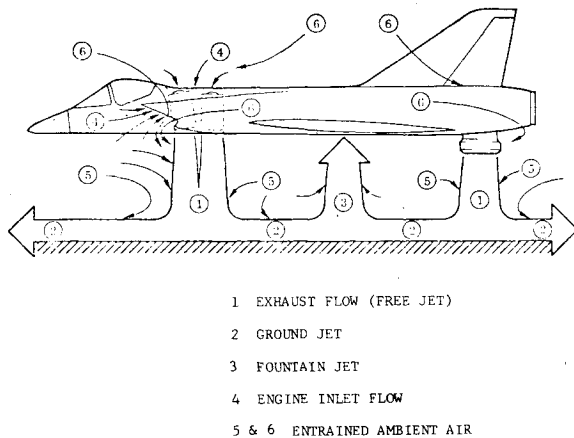


Fig. 1 Flowfields near a hovering VSTOL aircraft.

—fountain core associated lifting gains, ΔL_{FC} , and fountain interference effects, ΔL_{FI} . The net-induced force [Eq. (1)] is then modified.

$$(\Delta L/F_j) = (\Delta L_j/F_j) + (\Delta L_{FC}/F_j) + (\Delta L_{FI}/F_j) \quad (2)$$

Since the ultimate objectives of this research were the development of prediction techniques and an understanding of the physical-flow phenomena, the effects of varying the nozzle-exit conditions on the component forces described in Eq. (2) as well as on the net-induced force had to be determined.

Test and Model Description

The experimental investigation was conducted at the General Dynamics Fort Worth Division's Ground Effect Hover Test Facility. Testing consisted of three phases—a *nozzle calibration phase*, in which variations in nozzle exit conditions were determined; an *induced loads phase*, in which the net and component-induced forces produced by variations in model configuration (number of nozzles and blocking-surface planform shape), model altitude, and nozzle-exit conditions were measured; and finally, a *fountain survey phase*, in which the fountain-flow-field characteristics were investigated. Nozzle thrust and the planform-induced forces and moments were measured with individual 5-component strain-gage balances as indicated in Fig. 2. The rectangular and triangular, sharp 90 deg edge, flat-plate models of Ref. 10 (Fig. 3) were used to provide two-, three-, and four-nozzle configurations; in addition, a two-nozzle cruciform-blocking surface model, more characteristic of a realistic aircraft planform, was also investigated.

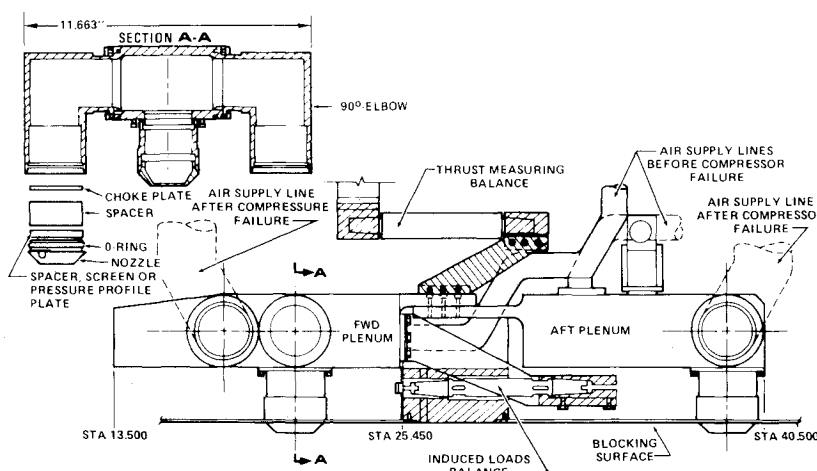


Fig. 2 A multi-purpose ground effects model was used.

Nozzle Calibration Phase

With the flat-plate planforms removed, nozzle thrust was measured for variations in nozzle size, nozzle-pressure ratio, nozzle-exit turbulence, and total pressure distribution. One of the test objectives was to cover the range of nozzle-exit flow parameters expected on real aircraft engines. To that end, nozzle-pressure ratios (NPR's) of 1.5, 2.0 and 2.4 were tested, and simulations of exit-pressure distributions and turbulence levels representative of turbojet and turbofan engines were obtained.

Turbulent intensity (I) was defined as the ratio of the area-weighted-average of the rms values of the fluctuating-total pressure across the nozzle exit to the area-weighted-average total pressure (gage) across the nozzle exit. The fluctuating-total pressure was measured by a high response subminiature-pressure transducer (Kulite) with an 0.08-in.-diam transducer face; the signal was fed through a true rms meter to provide an analog signal that was sampled at rates high enough and for long enough duration to ensure that, in the frequency ranges of interest (< 50 kHz), the total system error for intensity measurement was insignificant in terms of the objectives of this experiment. [The error in turbulent intensity measurement due to the nonlinear-frequency response characteristics of the Kulite transducer is reported by the manufacturer to be less than 3% for the turbulence-frequency range of this experiment (< 50 kHz) provided the turbulence-characteristic length (eddy size) is greater than the diameter of the Kulite transducer face (0.08 in.); as this length approaches the size of the transducer face, the error increases. Since the turbulence screen and pressure-profile plates used in this experiment all have characteristic lengths larger than the transducer face, the error in turbulent-intensity measurement for these cases is considered negligible ($< 10\%$). For the baseline-nozzle case (with choking plate), the eddy characteristic length is probably somewhat smaller than the transducer-face diameter and a significant error may be produced (with indicated readings too low). However, since the turbulence intensities are low for the baseline nozzle case ($< 10\%$), large percent errors in their measurement have little effect on the conclusions of this experiment.]

The upper limit of turbulence considered was guided by turbulent-intensity measurements of full-scale turbojet (Olympus 593) and turbofan (RB 211) engines measured with a laser velocimeter that gave 0.01 to 0.02 for the turbojet and, for the turbofan,¹² 0.01 in the core region and up to 0.20 in the fan region. Turbulent intensity variations on the model were achieved by placing turbulence generating screens S_1 and S_2 (Fig. 4) just upstream of the convergent nozzle section (Fig. 2). (The choke plate was always present well upstream within the nozzle body even for the baseline nozzle to provide uniform flow.)

Total-pressure-profile distributions were varied by placement of the P_1 or P_2 devices, shown in Fig. 4 upstream

Fig. 3 Large research and cruciform blocking surface models were used.

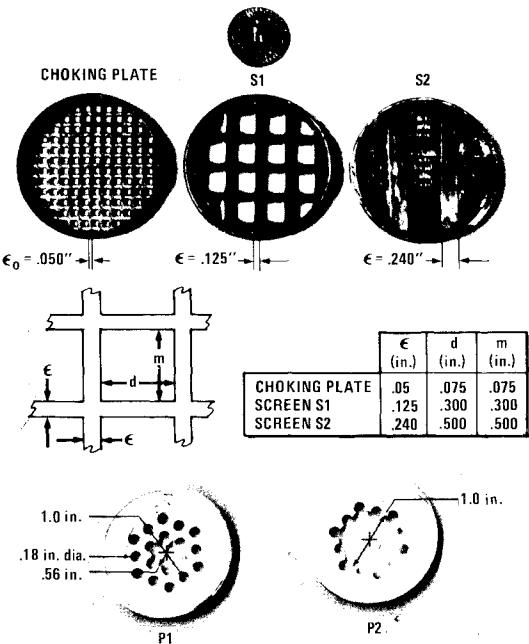
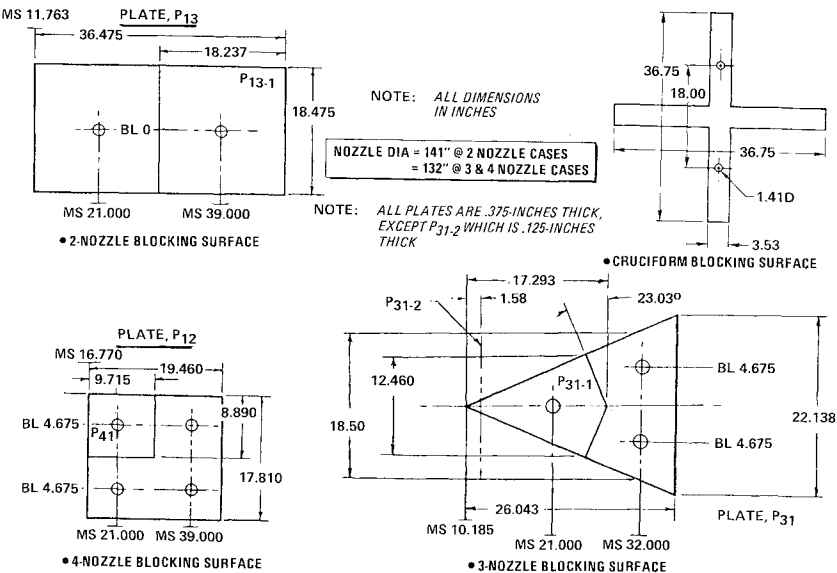


Fig. 4 The choking plate, screens S_1 and S_2 , and pressure-profile plates P_1 and P_2 provided the desired nozzle-exit turbulence and total-pressure distributions.

of the nozzle section. These devices plus the baseline nozzle allowed a simulation of turbofan and turbojet nozzle-pressure distributions. NPR is a somewhat arbitrary term when applied to nonuniform exit profiles like those produced by P_1 and P_2 . Therefore, the NPR's for the nonuniform profiles were taken as those measured on the baseline, "top hat" profiles when the thrust produced by the nonuniform profiles matched that of the baseline. The screens S_1 and S_2 produced virtually uniform profiles so no analogous difficulty was present.

Induced Loads Phase

The net induced lift force, ΔL , on the model planform was measured while varying configuration, nozzle-exit flow parameters, and model altitude. For the two-nozzle configuration, NPR's of 1.5, 2.0, and 2.4 were tested; three- and four-nozzle configurations were tested at an NPR of 2.0. The turbulence screens and pressure distribution plates were tested with the two- and four-nozzle configurations; screen variations only were tested with the three-nozzle configuration.

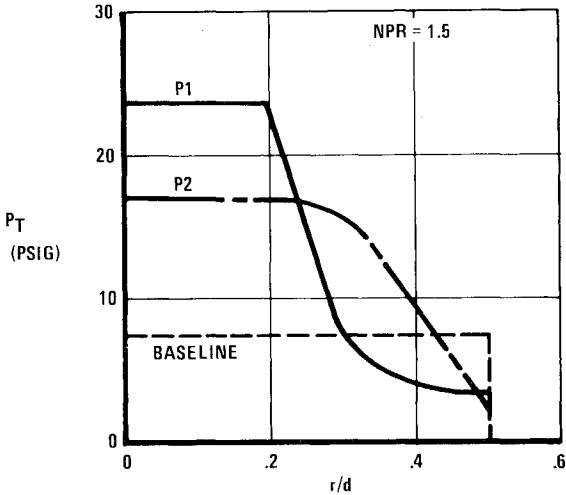


Fig. 5 Nozzle-exit total-pressure distributions characteristics of turbojet and turbofan engines were obtained with the baseline nozzle and plates P_1 and P_2 .

To determine the effects of varying nozzle-exit conditions on the pure suckdown component of the net-induced force, one-half of the two-nozzle plate was removed and the nozzle with the metric half of the plate was operated; induced loads were measured on the metric half-plate with the turbulence screens and pressure profile plates installed and with variations in model altitude. In all cases, model altitude was varied over h/D values from 2.5 to 10.0.

Fountain Survey Phase

A fountain rake with 14 cone pressure probes (4 statics plus 1 total pressure port per probe) was used with the two- and four-nozzle configurations at an NPR of 2.0 to ascertain the effects of the turbulence and pressure profile devices on the fountain-core force.

Results

Nozzle Calibration Phase

The baseline-nozzle configuration exhibits the classic "top hat" turbojet type uniform total-pressure distribution with a correspondingly low rms fluctuating-pressure level which is also uniform across the nozzle exit. Screens S_1 and S_2 also produce uniform rms and total-pressure distributions. Pressure-profile plates P_1 and P_2 successfully produced total-pressure distributions characteristic of turbofan engines of

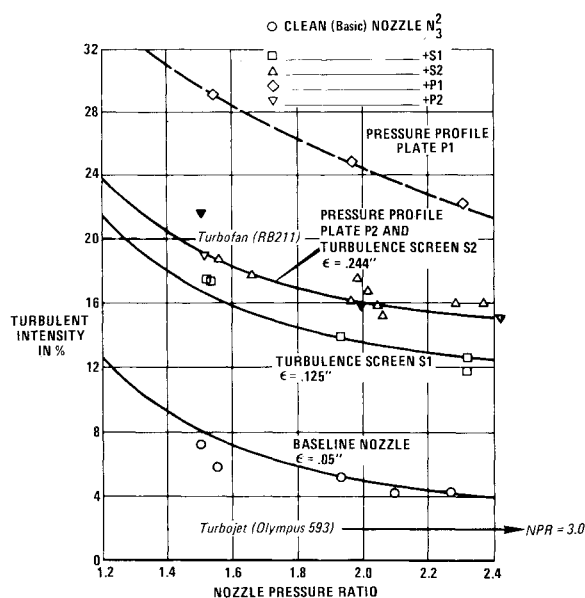


Fig. 6 The variation of turbulent intensity with NPR for screens and plates.

varying bypass ratio; pressure distributions for plates P_1 and P_2 at $NPR=1.5$ with the "top hat" profile of the baseline nozzle are shown in Fig. 5. Increases in rms pressure were also measured with P_1 and P_2 .

The variations in turbulent intensity with NPR calculated from the pressure surveys are shown in Fig. 6 and indicate that turbulent intensity can be changed in three ways: 1) by changing the base level with the screens while maintaining a uniform total-pressure distribution, 2) by distorting the total-pressure distribution with the plate devices, and 3) by changing the nozzle-pressure ratio. Within the accuracy of the data, the same variation in turbulent intensity with nozzle-pressure ratio occurs at all screen-grid sizes (including the choking plate of the baseline-nozzle case). The P_1 pressure plate exhibits a slightly different variation of I with NPR, but the trend is certainly the same as with the screens and P_2 .

Increasing the screen-grid size increases the turbulent intensity. The turbulence produced by the screen grid can be characterized by the large-scale eddy size, ϵ_e , (after Kolmogorof¹⁵) associated with the turbulence at the NPR. The large-scale eddy size is proportional to the largest physical dimension causing the turbulence, which, in the case of the screens, is taken as the width of the bars making up the screen grid ϵ ; ϵ is 0.05 in. for the choking plate of the baseline nozzle case, 0.125 in. for S_1 , and 0.240 in. for S_2 .

Kolmogorof's argument for a characteristic-turbulent large-scale eddy size leads to an estimate of the large-scale eddy size and the associated frequencies produced by the baseline nozzles and screens according to Eqs. (3) and (4).

$$\epsilon_p = \epsilon / 2\pi S \quad (3)$$

and

$$f = U / 2\pi \epsilon_e \quad (4)$$

where

S = Strouhal number = constant for flow past cylinders or plates^{13,14} taken as $S = 0.21$ for estimating ϵ_e

f = frequency of the large-scale eddies characterizing the turbulence.

U = constant velocity that is large compared to the turbulent perturbation velocity u' ; (U = nozzle exit velocity in this case)

Figure 6 also demonstrates that the ranges of turbulent intensities and NPR expected for full scale turbojet and turbofan engines have been adequately covered in the experiment; Rolls Royce laser-velocimeter-measured-turbulence levels are indicated for the RB211 turbofan engine and the Olympus 593 turbojet engine as mentioned above.





Induced Loads Testing

Variations of nozzle turbulence, nozzle pressure ratio, and nozzle total-pressure distributions do measurably affect not only the net induced forces $\Delta L/F_j$ but also the individual components of $\Delta L/F_j$ as defined by Eq. (2).

The maximum effect of the nozzle-exit variables on the net-induced forces for the two-, three-, and four-nozzle cases with the large-blocking surfaces are summarized in Table 1. Also included are the significant results obtained for the smaller cruciform-blocking surface more typical of a realistic aircraft planform. The amount of lift or thrust loss is very configuration dependent. In all cases, increasing turbulence increases the net-lift loss, but the magnitude of the loss is dependent on how turbulence is changed, whether by screen, nozzle-pressure ratio, or pressure distribution. Knowing the turbulent intensity alone is not enough to predict an airplane's performance; the nozzle-pressure ratio and pressure distribution are also important because they affect the manner in which the turbulence is developed.

The most significant result observed from the net-induced force testing is that when one goes to the smaller cruciform planform, more characteristic of a realistic airplane configuration, one still sees a 10% thrust loss due to increasing the turbulence (which was also observed with the large blocking surface), which is on the order of the airplane payload (Fig. 7). With the cruciform planform, the suckdown is considerably less than for the larger rectangular plate, but it is also evident that strong fountains are present. This is probably because the cruciform plate makes more surrounding air available for entrainment into the ground jets, which then requires less air to be entrained away from the fountain, resulting in a stronger fountain. Increasing the nozzle turbulence increases the entrainment of the free and

Table 1 Effects of nozzle exit variables on net-induced force, $\Delta L/F_j$

	Change in $\Delta L/F_j$			
				
	2 nozzle	3 nozzle	4 nozzle	Cruciform
Turbulence (with screens S_1 and S_2)	-0.078	-0.032	-0.021	-0.072
Nozzle pressure ratio (1.5-2.4)	+0.04	-	-	-
Nozzle total pressure profile (with plates P_1 and P_2)	-0.05	-	-0.024	-

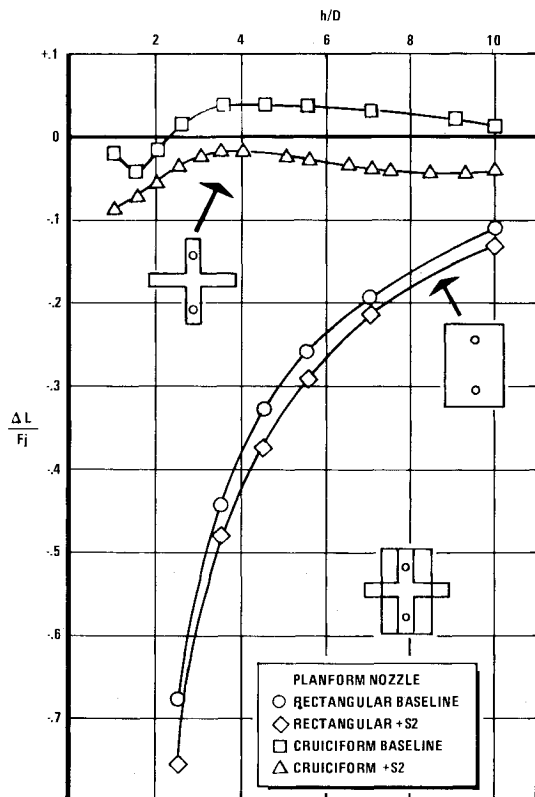


Fig. 7 Real aircraft engine turbulence levels cause large changes in ground effects for aircraft and research-type blocking surfaces.

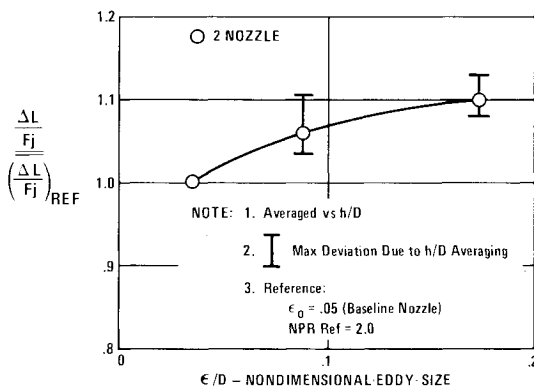


Fig. 8 Effect of varying nozzle exit turbulence with screens on net-induced force for two-nozzle case.

ground jets, which in turn decreases the fountain strength—both of which contribute to a more negative net-induced force.

The independent effects on the net induced forces of varying turbulence by changing the base level with the screen-grid size or by changing the NPR have been developed for the two-nozzle large rectangular blocking surface case (Figs. 8 and 9) in the work by Foley.¹⁶ Increasing the screen grid or eddy size produces an increased suckdown; increasing NPR produces a substantial reduction in suckdown.

The concept of the turbulent-eddy size to explain the increased suckdown obtained with the screens and NPR variations is useful. The Kolmogorof energy dissipation rate ϵ for turbulence scaled by eddy size is related to U^3 .¹⁵ Foley postulates¹⁶ that, for a given NPR, as eddy size is increased, turbulent intensity increases and the energy dissipation rate decreases, providing higher-energy large eddies for entraining surrounding air and therefore increasing suckdown. For a given eddy size, as NPR (which is proportional to U^2 up to $NPR_{critical}$) is increased, the dissipation rate increases, reducing the energy in the large eddies for entrainment and thereby reducing suckdown. At choked and superchoked conditions, NPR is not proportional to U^2 , and the effect of varying NPR on eddy size is much degraded, as noted in Fig. 6.

However, replacing turbulent intensity with eddy size (or the characteristic length producing the eddy size) as the key variable presupposes that the effective-eddy size of the full-scale engine can be estimated by knowing the size of the turbulence-producing parts of the engine (say turbine blade size). This remains to be determined. It may be easier to continue to measure the model and full-scale engine turbulent-intensity levels and apply appropriate corrections to the model-scale nozzle-exit conditions in the model ground effects test.

Effects on Component Forces

Table 2 summarizes the maximum effects observed on the component forces due to varying the nozzle exit conditions.

Foley demonstrated¹⁶ that, like the net-induced force, varying the NPR causes different (independent) changes in the pure suckdown that are produced by changing the turbulence screens (Fig. 10); these changes may be correlated as a function of the screen-grid size ϵ which, as indicated above, is related to the turbulence large-eddy size ϵ_e [Eq. (3)].

Estimates of the fountain core force $\Delta L_{FC}/F_j$ were determined by integrating the vertical component of the fountain dynamic pressure measured by three-dimensional surveys with the 14-cone pressure-probe fountain-flow rate for the two- and four-nozzle cases; the nozzle turbulence was varied with screen S_2 and pressure-profile plate P_2 at a constant NPR of 2.0. The results are plotted as a function of

Table 2 Maximum effect of varying nozzle exit conditions on component forces

$\Delta L/F_j$ net induced force	Change in component		
	$\Delta L_j/F_j$ pure suckdown	$\Delta L_{FC}/F_j$ fountain core	$\Delta L_{FI}/F_j$ fountain interference
Turbulence (with screens S_1 and S_2)	-0.07	Two nozzle 0 (0) Four nozzle -0.01	Two nozzle -0.015 Four nozzle -0.024
Nozzle pressure ratio (1.5-2.4)	+0.04 Assumed same as for $\Delta L/F_j$	-	-
Nozzle total pressure distribution (with plates P_1 and P_2)	-0.04	Four nozzle -0.007	Two nozzle -0.03

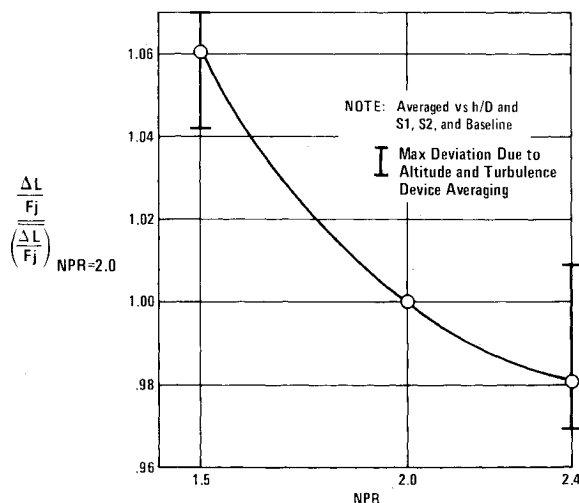


Fig. 9 Effect of varying NPR on net-induced force for two-nozzle case.

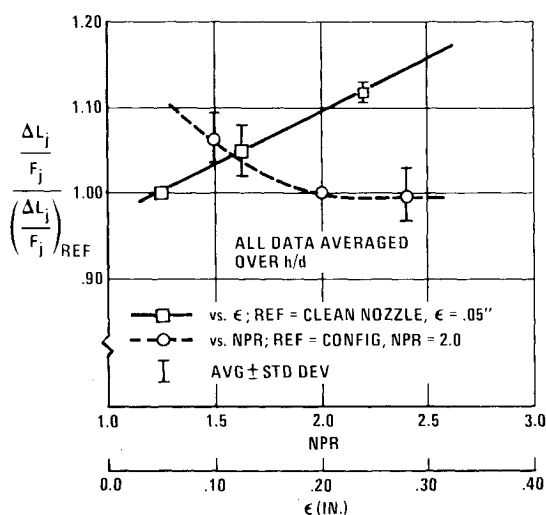


Fig. 10 Effect of nozzle exit-pressure ratio and turbulence scale on pure suckdown.

the nondimensionalized rake height above the ground (Z/D) in Fig. 11. The weak fountain formed beneath the large rectangular planform two-nozzle configuration dissipated before it reached the blocking surface as a result of the entrainment of air away from the fountain by the free and radial-ground jets which reduces the fountain momentum to zero at the blocking surface for the altitudes investigated. Figure 11 also demonstrates that increasing the nozzle turbulence does reduce the fountain core force by increasing the freejet and ground jet entrainment, resulting in even more air entrained away from the fountain. The stronger-fountained four-nozzle configuration does not dissipate before reaching the blocking surface at an h/D of 5.0 or 8.0. Increasing the nozzle turbulence causes a reduction in fountain-core force; varying the total-pressure distribution also changes the fountain core force. Increasing the blocking surface height yields a stronger fountain for the same degree of nozzle turbulence. For a constant blocking-surface height, the fountain dissipates at increasing altitudes and at a rate that is virtually independent of nozzle turbulence.

The effect of varying the nozzle-exit conditions on the fountain interference force, $\Delta L_{FI}/F_j$, on the two- and four-nozzle configurations at an NPR of 2.0 was determined (Fig. 12) by subtracting the pure suckdown and fountain-core force increments from the net-induced forces. At almost all altitudes, increasing the nozzle exit turbulence with the

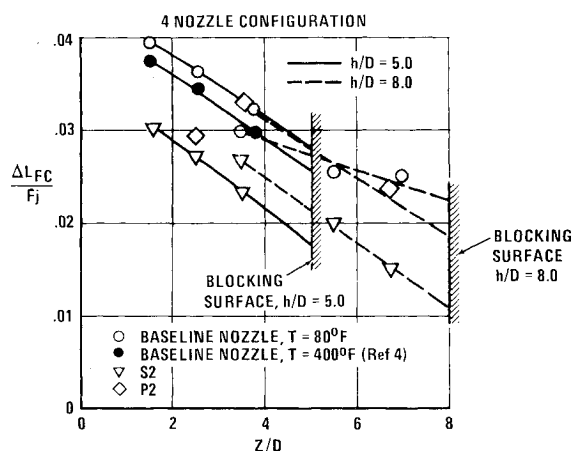
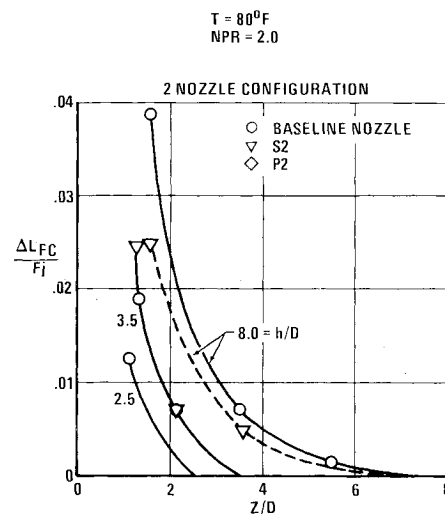


Fig. 11 Effect of varying nozzle turbulence (screens) and pressure distribution on fountain-core force.

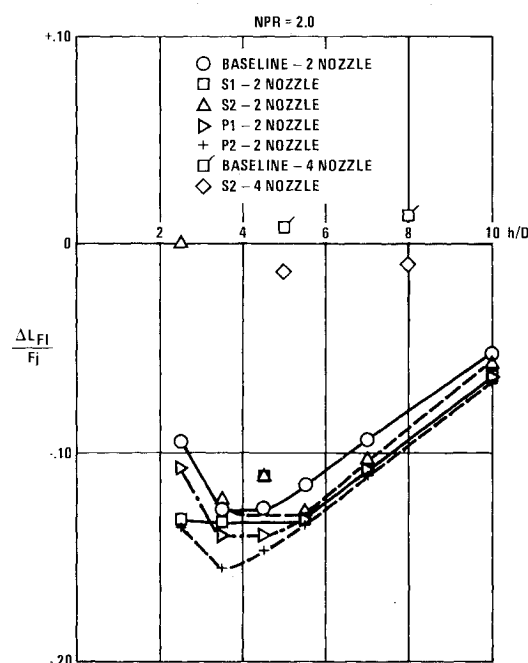


Fig. 12 Increasing nozzle turbulence or varying the nozzle-pressure distribution degrades fountain interference, $\Delta L_{FI}/F_j$.

screens or pressure profile plates at a constant NPR causes a suckdown—increasing fountain interference effect.

Conclusions

This investigation has successfully demonstrated the criticality of engine-exhaust simulations on model-measured ground effects. The results have formed the basis of prediction techniques to account for these effects and have provided some understanding of the associated flow phenomena.

1) Variations in nozzle exit turbulence, total-pressure distribution, and nozzle-pressure ratio have been experimentally demonstrated over the ranges expected for full-scale VSTOL aircraft turbojet and turbofan engines.

2) Increasing nozzle turbulence increases net lift or thrust loss, but the magnitude of the loss is dependent on the configuration and how the turbulence is changed, whether by screen, nozzle-pressure ratio, or pressure distribution. Turbulence may be increased by increasing the large-scale eddy size with screens while maintaining a virtually uniform total-pressure distribution, by varying the total-pressure distribution from that of a turbojet to a turbofan engine, or by decreasing NPR.

3) Because the net-induced force is often the sum of two relatively large-valued forces of opposite sign (suckdown and fountain lift), changes on the order of 10% in the suckdown and fountain force could potentially result in first-order changes in aircraft sizing and performance and must therefore be accounted for in any prediction methodologies.

4) The effect of the nozzle exit variables on the net induced force is highly configuration dependent. When the large research-type blocking surface is changed to a smaller cruciform planform, more characteristic of a realistic airplane configuration, varying the nozzle exit conditions still produces a 10% thrust loss, which is on the order of the airplane payload. Therefore, if the effects of the nozzle-exit conditions of the engines expected for use on VSTOL airplanes are not considered, costly errors in airplane sizing will result.

5) The induced loads and fountain-survey measurements have led to the following explanation of the flow phenomena observed with changing nozzle-exit conditions. The induced forces for a configuration are largely a function of the entrainment by the free and radial-ground jets. The entrainment of the free and radial-ground jets may be increased by increasing the nozzle-exit turbulent-eddy size or by decreasing the NPR, probably resulting in slower energy dissipation by the eddies and higher energy eddies for entrainment.

When turbulence levels like those measured for real engines are introduced at the nozzle exit, the entrainment rate of the free and radial-ground jets is increased, which results in more air being entrained away from the fountain, in higher suckdown pressures, and in reduced fountain-core strength.

References

- ¹Gentry, G.L. and Margason, R.J., "Jet-Induced Lift Losses on VTOL Configuration Hovering In and Out of Ground Effects," NASA TN D-3166, Feb. 1966.
- ²Kuhlman, J.M. and Warcup, R. W., "Effect of Jet Decay Rate on Jet-Induced Loads on a Flat Plate," *Proceedings of the AIAA/NASA Ames VSTOL Conference*, June 1977, p. 194.
- ³Bradbury, L.J.S., "The Impact of an Axisymmetric Jet Onto a Normal Ground," *Aeronautical Quarterly*, May 1972.
- ⁴Wyganski, O. and Fielder, H., "Some Measurements in the Self-Preserving Jet," *Journal of Fluid Mechanics*, Vol. 38, Pt. 3, Sept. 1969, pp. 557-612.
- ⁵Krenz, G., Haftmann, R., Brennan, T., and Fortenbaugh, R., "USN/FMOD FRG VAK-191B Joint Flight Test Program, Vol. 8," Naval/Air Systems Command Rept. NACAIR-8R-76, Aug. 1976.
- ⁶Kontansky, D.R., Durando, N.A., and Bristow, D.R., "Jet-Induced Forces and Moments In and Out of Ground Effect," McDonnell Aircraft Company Rept. NADC-77-229-30, July 1977.
- ⁷Sicliari, M.J., Barche, J., and Migdal, D., "V/STOL Aircraft Prediction Technique Development for Jet-Induced Lift in Hover," Grumman Aerospace Corporation Rept. PDR 623-18, April 1975.
- ⁸Karemaa, A. and Ramsey, J.C., "Aerodynamic Methodology for the Prediction of Jet-Induced Lift in Hover," Convair Rept. CADS-ERR-73-013, Dec. 1973.
- ⁹Karemaa, A., "Abbreviated Methodology for the Prediction of Jet-Induced Lift in Hover," Convair Rept. CADS-ERR-74-024, Dec. 1974.
- ¹⁰Karemaa, A., Smith, C.W., Weber, H.A., and Garner, J.E., "The Aerodynamics and Thermodynamic Characteristics of Fountains and Some Far-Field Temperature Distributions," Office of Naval Research Rept. ONR-CR-212-237-1, May 1978.
- ¹¹Karemaa, A., Weber, H.A., and Smith, C.W., "Aerodynamic and Thermodynamic Characteristics of Flow Below VTOL Vehicles in Ground Proximity," AIAA Paper 79-0338, New Orleans, La., Jan. 1979.
- ¹²Smart, A.E. and Moore, C.J., "Aero-Engineer Applications of Laser Anemometry," *AIAA Journal*, Vol. 14, March 1976, pp. 363-370.
- ¹³Schlichting, H., *Boundary-Layer Theory*, Chap. II, McGraw Hill, New York, 1968.
- ¹⁴Hoerner, S.F., *Fluid Dynamic Drag*, Chap. III, Hoerner, Midland Park, N.J., 1965.
- ¹⁵Landau, L.D. and Lifshitz, G.M., *Fluid Mechanics*, Chap. III, Pergamon Press, London, 1966.
- ¹⁶Foley, W.H., "Development of an Experimental Basis for a V/STOL Handbook," *Proceedings of the Workshop on V/STOL Aerodynamics*, Monterey, Calif., May 1979, pp. 276-292.